PCCP

ROYAL SOCIETY OF CHEMISTRY

PERSPECTIVE

View Article Online
View Journal | View Issue

Cite this: *Phys. Chem. Chem. Phys.*, 2024, **26**, 713

Understanding the "Berg limit": the 65° contact angle as the universal adhesion threshold of biomatter

Matej Kanduč, *[a] Emanuel Schneck [b] and Roland R. Netz [c]

Surface phenomena in aqueous environments such as long-range hydrophobic attraction, macromolecular adhesion, and even biofouling are predominantly influenced by a fundamental parameter—the water contact angle. The minimal contact angle required for these and related phenomena to occur has been repeatedly reported to be around 65° and is commonly referred to as the "Berg limit." However, the universality of this specific threshold across diverse contexts has remained puzzling. In this perspective article, we aim to rationalize the reoccurrence of this enigmatic contact angle. We show that the relevant scenarios can be effectively conceptualized as three-phase problems involving the surface of interest, water, and a generic oil-like material that is representative of the nonpolar constituents within interacting entities. Our analysis reveals that attraction and adhesion emerge when substrates display an underwater oleophilic character, corresponding to a "hydrophobicity under oil", which occurs for contact angles above approximately 65°. This streamlined view provides valuable insights into macromolecular interactions and holds implications for technological applications.

Received 19th October 2023,
Accepted 8th December 2023

DOI: 10.1039/d3cp05084j

rsc.li/pccp

1 Introduction

Interactions among macromolecules, proteins, cells, and large surfaces in liquids have been a topic of extensive scientific inquiry, driven by their significance across a diverse spectrum of disciplines. Early on, it became clear that factors influencing processes such as protein adsorption and cellular adhesion are multifaceted, encompassing physical, chemical, and biological aspects.[1–3] Understanding the mechanisms of molecular adsorption is crucial for various applications, ranging from coating technologies[4–6] and anti-biofouling strategies[7] to biomedical implants[8] and drug delivery.[9,10] For instance, achieving biocompatibility of artificial implants and regulating the adsorption of proteins at their surfaces are crucial factors that significantly influence the functionality and long-term performance of these materials.[8,11,12]

Despite the complex and structure-specific nature of these interactions,[1] there is a universal water-mediated component associated with the hydrophobicity of the interacting interfaces. The hydrophobicity is reflected in the surface contact angle and gives rise to two contrasting behaviors. One end features highly polar, hydrophilic surfaces, characterized by a small or even vanishing contact angle. Such surfaces repel each other at close distances (below about 2 nm) because of tightly bound water molecules—an effect known as *hydration repulsion*.[13–15] At the opposite end of the spectrum, nonpolar, hydrophobic surfaces with large contact angles attract one another in a water environment *via* very long-range interactions (up to ≈100 nm), mediated by surface nanobubbles.[1,16]

This dichotomy raises a fundamental question: where does the transition from attraction to repulsion exactly occur? Or, in other words, above which threshold contact angle, θ_{adh}, does a surface begin to display adhesion? This question was addressed in a seminal paper by Vogler in 1998.[17] Combining various experimental data, he identified a critical contact angle of approximately 65° for which he coined the term "Berg limit" after the researchers who first encountered this value.[18] Since its publication, Vogler's work has had a profound impact, particularly in the fields of macromolecular adsorption, cell settlement, and biofouling.[12,19–21] Fig. 1a shows an example of how protein adsorption and cell settlement dramatically ramp up once the contact angle of the substrate surpasses a value of around 65°. This transition in adhesion propensity has far-reaching consequences for biological responses to biomaterials (*e.g.*, bioadhesion, protein adsorption, blood plasma coagulation, and immune response), which undergo a marked shift at contact angles of around 65°.[17,22–25] This contact angle has even

[a] *Department of Theoretical Physics, Jožef Stefan Institute, Jamova 39, SI-1000 Ljubljana, Slovenia. E-mail: matej.kanduc@ijs.si*
[b] *Department of Physics, Technische Universität Darmstadt, Hochschulstrasse 8, Darmstadt 64289, Germany*
[c] *Fachbereich Physik, Freie Universität Berlin, Arnimallee 14, Berlin 14195, Germany*

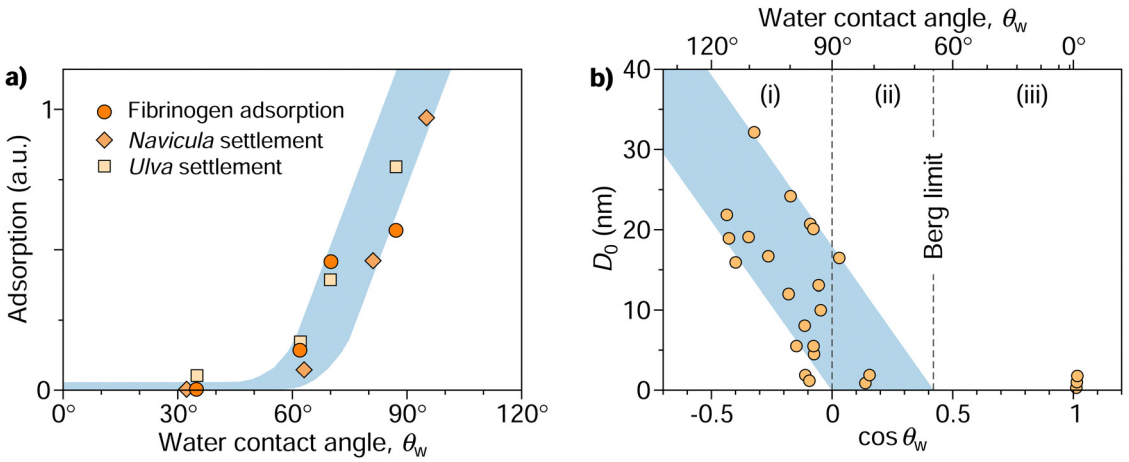

Fig. 1 (a) Protein (fibrinogen) adsorption and settlement of algae cells (*Navicula* and *Ulva* zoospores) on a series of oligo(ethylene glycol) terminated self-assembled monolayers characterized by different contact angles.[32,33] Re-plotted from Rosenhahn *et al.*[33] with permission from the Royal Society of Chemistry. (b) Compilation of characteristic decay lengths (D_0) extracted from experimental force–distance data of various systems plotted against the cosine of water contact angles of interacting surfaces. Re-plotted from Vogler[17] with permission from Elsevier. The diagram features three distinct regimes of surface interactions: (i) long-range attraction between hydrophobic surfaces, (ii) shorter-range attraction between some of the hydrophilic surfaces with contact angles down to the Berg limit, and (iii) absence of attraction beyond the Berg limit.

been proposed as a new criterion for classifying surfaces as hydrophobic or hydrophilic,[26–28] offering an alternative to the more traditional and widely accepted threshold of 90°.[29] Despite the growing recognition of the critical adhesion contact angle, a fundamental understanding of its underlying principles remains elusive, even a quarter-century since its initial introduction.

In the present article, we first briefly review the experiments that led to the concept of a universal contact angle threshold, discuss the current knowledge on this topic, and revisit our past research endeavors dedicated to this question. Subsequently, we propose a novel perspective by recognizing that non-polar hydrocarbon-based matter, a ubiquitous component of biological and soft-matter systems, can provide additional interaction mechanisms in aqueous systems. By analyzing several basic scenarios, we demonstrate that the phenomena of attraction and adhesion distinctly manifest once the contact angle surpasses a well-defined critical threshold. Importantly, this threshold closely aligns with the "Berg limit," which has been identified in experimental studies.

2 State of the art and current understanding

2.1 Long-range hydrophobic attraction

Following the pioneering experiments by Israelachvili and Pashley in the early 1980s using the surface force apparatus,[30,31] it has become evident that the attraction between large hydrophobic surfaces cannot be rationalized by van der Waals interaction alone but is more intricate and multifaceted than initially presumed. The measurements of these apparent "hydrophobic forces" revealed that they operate over a considerably long range (tens or even hundreds of nanometers) and exhibit an approximately exponential decay with the surface separation (D), occasionally in a step-wise fashion.[1,16] This decay is characterized by a specific decay length denoted as D_0, thus following the form $\exp(-D/D_0)$.

Vogler[17] compiled measurements from different experiments and noted the general trend that D_0 correlates with the water contact angle of the surfaces, θ_w. Fig. 1b, a slightly modified version of Vogler's original plot, shows D_0 over $\cos\theta_w$ for all collected measurements. The decay length ramps up for hydrophobic surfaces with contact angles above 90° (corresponding to $\cos\theta_w < 0$). When fitting the lower bound of the rather scattered data points, one finds convergence to a contact angle of 90° as D_0 approaches 0. Meanwhile, the fit of the upper bound reaches zero at a contact angle of approximately 65°, a value termed the "Berg limit" by Vogler,[17] in reference to Berg *et al.*,[18] who were the first to report the absence of attraction below this contact angle in Langmuir–Blodgett films. More precisely, Vogler proposed a range of the *water adhesion tension*, $\gamma_w \cos\theta_w$, between 20 and 40 mN m^{-1} as the onset of attraction, corresponding to a contact angle window of 56°–74°. The midpoint of this interval, θ_{adh} = 65°, which we will refer to as the *adhesion threshold*, has gained broad acceptance and has become a consensus value of the boundary for adhesion in the literature.[11,19,21,27,28]

The data in Fig. 1b indicate three distinct regimes: (i) surfaces with contact angles above 90° without exception exhibit long-range attractive forces, with a range that tends to grow with increasing contact angles. (ii) As the contact angle drops below 90°, fewer surfaces exhibit long-range attraction until reaching the critical contact angle $\theta_{adh} \approx 65°$, below which attraction becomes undetectable (iii). What mechanisms are behind these three regimes, and what determines the specific values of 65° and 90°? Previous hypotheses suggesting that long-range attraction originates from varying "structures" of water extending tens of nanometers from

its interface[17] have been disproven. Although water does undergo structural changes, loses hydrogen bonds, and exhibits increased fluctuations near nonpolar surfaces, these alterations are confined to only a few water layers from the interface[34–37] and thus cannot explain the observed long-range attraction.

2.2 Attraction between hydrophobic surfaces ($\theta_w > 90°$)

The apparent long-range attraction, particularly for hydrophobic surfaces with $\theta_w > 90°$, is nowadays pretty well understood.[38–44] Its origin lies in the thermodynamic instability of the water slab between two hydrophobic surfaces against cavitation to a vapor phase.

To provide a quick overview of the underlying thermodynamics, consider two extensive parallel surfaces of area A characterized by the contact angle θ_w and separated by a distance D. In the continuum description, the free energy difference between the hydrated state (with liquid water between the surfaces) and the cavitated state (with water vapor between the surfaces) is $\Delta W = 2A(\gamma_{sv} - \gamma_{sw}) + pV$. The first term is related to the difference in the surface free energies, where γ_{sv} and γ_{sw} are the surface–vapor and surface–water surface tensions, respectively. The second term represents the work required to expel the water slab of volume $V = AD$ into the bulk against the ambient pressure p. Note that we have neglected the small vapor pressure and the energy of the water–vapor interface at the perimeter of the cavity. Using the Young equation [eqn (7) later on], one arrives at[45]

$$\Delta W/A = 2\gamma_w \cos\theta_w + pD \quad (1)$$

The cavitated state is thermodynamically favorable ($\Delta W < 0$) for separations below a critical distance $D_c = -2\gamma_w \cos\theta_w/p$, which exists only for contact angles above 90°. Hence, the use of a 90° contact angle as the boundary between hydrophilic and hydrophobic surfaces is not merely a geometric differentiation based on wetting properties of a single surface; it is grounded on fundamental physical principles governing the stability of liquid aqueous films between surfaces. For a prototypical hydrophobic surface with $\theta_w = 120°$ at atmospheric conditions ($p = 1$ bar) the critical distance is $D_c \approx 720$ nm. In the cavitated state, the surfaces attract each other because of several factors: the capillary forces at the perimeter of the cavity, van der Waals forces between the surfaces across vapor (which are stronger than those in water), and the external atmospheric pressure. Namely, the cavity contains water vapor and, for relevant timescales, is not in chemical equilibrium with the atmosphere. The cavitation (drying) transition has also been observed in atomistic simulations of smaller systems, such as narrow hydrophobic slits[46–48] and pockets.[49,50]

However, the cavitation transition of larger systems is associated with the nucleation of a vapor bubble that spans across both surfaces. The free energy required to nucleate such a bridging bubble scales quadratically with separation, $\Delta W^* \sim \gamma_w D^2$,[37,45,46,51,52] although linear terms stemming from line tension may become important at small separations.[48,52] This free energy represents the kinetic barrier the system needs to overcome in order to cavitate. On experimental time scales, a macroscopic system is capable of overcoming a barrier of the order of $\Delta W^* \sim 10\text{–}100 k_B T$, where $k_B T$ is the thermal energy (with k_B being the Boltzmann constant). Thus, one can anticipate that the cavitation-induced attraction in contaminant-free water will occur spontaneously only at distances below around $D_{cav} \sim (\Delta W^*/\gamma_w)^{1/2} \approx 1\text{–}2$ nm. This value is 3 orders of magnitude below D_c and 1–2 orders of magnitude smaller than the reported characteristic decay lengths D_0 of measured hydrophobic forces (see Fig. 1b). However, in cautiously conducted experiments that avoid contamination and pre-existing gas bubbles, the metastable water-filled state, characterized by the absence of attraction, is indeed observed down to a few nanometers of separation before the jump into close contact occurs.[1,53,54] Quite often, cavitation, and with that the apparent hydrophobic attraction, is catalyzed by various kinds of impurities, most notably pre-existing surface nanobubbles.[1] Long-lived nanobubbles residing on surfaces have been first postulated by Parker *et al.*,[16] based on the step-wise nature of their force–distance curves, and have been experimentally observed a few years later by atomic force microscopy (AFM).[55–57] The long-lived stability of surface nanobubbles seemed paradoxical at first, since classical theory predicts that gas bubbles cannot achieve stable equilibrium and should immediately dissolve because of a high Laplace pressure.[58] However, this paradox has finally been resolved in recent years.[59–62]

In summary, the measured long-range attraction between hydrophobic surfaces is not an inherent water-mediated interfacial force in the usual sense. Instead, it is a composite phenomenon driven by cavitation and is best understood in terms of the free energy of thermodynamic states of the two surfaces immersed in water. The gaseous capillary bridges resulting after cavitation engender a directly measurable attractive force in experiments. Consequently, the decay length D_0 is not an elementary water or material property but rather a parameter influenced by intricate experimental details, such as water purity, the concentration of dissolved gases, and, most notably, the pre-existence and distribution of surface nanobubbles. Hence, while Vogler's plot (Fig. 1b) does not represent a fundamental law but rather a compilation of empirical data, it stands as a visionary work that forged a link between attraction/adhesion and the contact angle, shedding valuable light on the subject.

2.3 Attraction between hydrophilic surfaces ($\theta_w < 90°$)

While we understand considerably well why hydrophobic surfaces with contact angles above 90° experience long-range attraction, as outlined above, the puzzle persists as to why some hydrophilic surfaces also attract, albeit more weakly, and form stable adhesion states, for contact angles way down to around $\theta_{adh} = 65°$.[18,63–66] In our previous theoretical studies[67–69] supported by all-atom molecular dynamics (MD) simulations, we explored an entire spectrum of model surfaces, ranging from hydrophobic to highly hydrophilic. We found that weakly hydrophilic surfaces can indeed form stable adhesion (close-contact) states without any intervening water layer, a phenomenon that we termed *dry adhesion*. In the following,

we briefly summarize the main concept behind this "hydrophilic attraction". The adhesion free energy, ΔW, between two surfaces immersed in water can be conceptualized as the result of a two-step process: in the first step, we remove the water between the surfaces, similar to the cavitation process described before, requiring the work of $2A\gamma_w \cos\theta_w$. In the second step, we bring the two surfaces into close contact, and thereby gain the work of adhesion, Aw_{ss}, between these two surfaces across vacuum (or vapor), where w_{ss} is the direct surface–surface adhesion tension (free energy per unit area). It should be noted that in this case, we have omitted the pV term because there is no net change in volume. Summing up the two components yields the *adhesion free energy* in water, representing the difference in free energy between the state where the two surfaces are in close and dry contact and the state where they are significantly separated across water,

$$\Delta W/A = 2\gamma_w \cos\theta_w - w_{ss} \quad (2)$$

When the surfaces are sufficiently hydrophilic and the first term predominates, they will experience hydration repulsion ($\Delta W > 0$) at close contact, as was shown earlier.[67] If they are less hydrophilic, such that the second term predominates, or even hydrophobic, such that both terms are negative, they will favorably adhere to each other ($\Delta W < 0$).

However, in practice, the two terms are not independent of each other, as they are primarily influenced by the chemical groups present at the interfaces. Groups with greater polarity (having larger electric dipoles) lead to lower contact angles θ_w[69] (*i.e.*, larger $\cos\theta_w$) and, at the same time, also to higher direct surface–surface interaction, w_{ss}. Thus, we can consider $w_{ss}(\theta_w)$ a function of θ_w. The critical contact angle, θ^*_{adh}, that marks the onset of dry adhesion ($\Delta W = 0$) can be expressed as

$$\cos\theta^*_{adh} = \frac{w_{ss}(\theta^*_{adh})}{2\gamma_w} \quad (3)$$

Its value is determined by the specific behavior of $w_{ss}(\theta_w)$. For two non-crystalline surfaces with liquid-like properties, which optimize contacts when in close proximity, estimating the lower bound of w_{ss} is rather simple: the weakest attraction is experienced between nonpolar or oil-like surfaces, where w_{ss} corresponds to the free energy of forming two interfaces of hydrocarbon-based oil in air with surface tension γ_o. In this case $w_{ss} \approx 2\gamma_o$. Rendering a surface more polar, for example by functionalization with hydroxyl (OH) groups, increases the direct attraction, such that $w_{ss}(\theta) \geq 2\gamma_o$. By incorporating this insight into eqn (3), we establish the upper bound of θ^*_{adh} for soft surfaces

$$\cos\theta^*_{adh} \geq \frac{\gamma_o}{\gamma_w} \quad (4)$$

With $\gamma_o \approx 25$ mN m^{-1} for a typical hydrocarbon oil surface tension,[70] the adhesion contact angle is constrained to $\theta^*_{adh} \lesssim 70°$. The precise value of θ^*_{adh} depends on various surface details, but these variations tend to be relatively tiny. In our simulation study,[69] where we analyzed the relation $w_{ss}(\theta_w)$ of vastly different surface models, we found a range of $\theta^*_{adh} = 40° - 84°$. The midpoint of this range closely coincides with the experimentally reported value of $\theta_{adh} = 65°$.[17] It turns out that at the adhesion threshold, the surfaces exhibit a notable lack of polarity, aligning them closely with the typical characteristics associated with oils. Consequently, the threshold value θ^*_{adh} is often close to the upper bound of eqn (4). For rigid, crystalline surfaces that cannot readily optimize their mutual contacts when in close proximity, w_{ss} may be marginally reduced. This results in a slightly elevated threshold for θ^*_{adh}, which explains why values up to 84° were obtained in the simulations.[69]

While the conclusions drawn from MD simulations lend support to the idea that hydrophilic surfaces with contact angles between θ^*_{adh} and 90° can indeed attract and form stable adhered states, it is essential to note that this hydrophilic attraction is remarkably short-ranged, limited to distances below a nanometer.[67–69] This observation is by itself not unexpected, given the fact that the alterations in water structure are limited to just a few water layers from the interface.[34–37] What thus remains unclear is why attraction in experimental studies was reported to range over several or even tens of nanometers.[64–66] This conundrum shares similarities with hydrophobic surfaces, which, under ideal conditions, cannot undergo cavitation transition when separated by more than a few nanometers. As mentioned, in those cases, the presence of another component—surface nanobubbles—is necessary to initiate the process. However, contrary to hydrophobic surfaces, hydrophilic surfaces ($\theta_w < 90°$) do not facilitate spontaneous cavitation, and any pre-existing gas nanobubbles compressed between such surfaces would result in repulsion rather than attraction.[71] This suggests that the mechanism for long-range hydrophilic attraction presumably involves another component.

In reality, aqueous environments are never entirely free of impurities.[72] In addition to dissolved gasses and stable nanobubbles, aqueous systems often contain varying quantities of insoluble hydrophobic and amphiphilic substances that can form oil-like aggregates. This is particularly evident in biological fluids, where the traits of soft and fluid hydrocarbon-based materials bear similarities to those of oils. In subsequent sections, we will delve into how these factors introduce additional attractive interaction mechanisms above a critical contact angle.

3 Water–oil–surface wetting

In this section, we recap the basics of oil and water wetting of solid surfaces by considering three different scenarios, shown in Fig. 2: (a) a water droplet on a solid surface in air, (b) an oil droplet on a solid surface in air, and (c) an oil droplet on a solid surface in water. The Young equations corresponding to these scenarios are

$$\cos\theta_w = \frac{\gamma_{sv} - \gamma_{sw}}{\gamma_w} \quad \text{(water droplet in air)} \quad (5)$$

$$\cos\theta_o = \frac{\gamma_{sv} - \gamma_{so}}{\gamma_o} \quad \text{(oil droplet in air)} \quad (6)$$

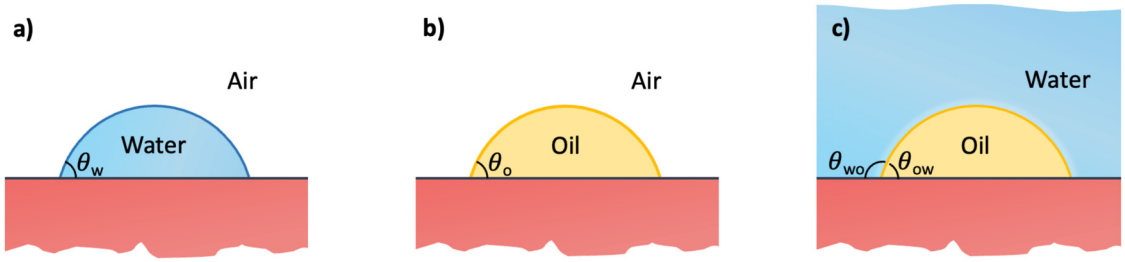

Fig. 2 Sessile droplets on a solid surface. (a) Water droplet in air, characterized by the water (w) contact angle θ_w. (b) Oil droplet in air, characterized by the oil (o) contact angle θ_o. (c) Oil droplet in water, characterized by the oil-in-water (o/w) contact angle θ_{ow}. The latter is related to the water-in-oil (w/o) contact angle θ_{wo} *via* the relation $\theta_{wo} + \theta_{ow} = 180^\circ$.

$$\cos\theta_{ow} = \frac{\gamma_{sw} - \gamma_{so}}{\gamma_{ow}} \quad \text{(oil droplet in water)} \tag{7}$$

where "o" stands for oil, "w"' for water, "s" for the solid surface/substrate, and "v" for vacuum/vapor/air. Note that the inverted version of the third scenario, with a water droplet in an oil phase, is straightforward as the oil-in-water (o/w) and the water-in-oil (w/o) contact angles are supplementary, $\theta_{wo} + \theta_{ow} = 180^\circ$. By combining the above equations and eliminating surface tensions related to the solid surface, we express the o/w contact angle as

$$\cos\theta_{ow} = \frac{\gamma_o\cos\theta_o - \gamma_w\cos\theta_w}{\gamma_{ow}} \tag{8}$$

This relation, also known as the Bartell–Osterhof equation,[73] predicts the contact angle between two immiscible liquids, θ_{ow}, based on the known contact angles of each liquid in air. In eqn (8), the characteristics of the solid surface come into play indirectly, through the two contact angles in air (θ_o and θ_w). As the surface polarity increases (*e.g.*, by functionalization with polar chemical groups), the water contact angle θ_w decreases. In contrast, θ_o is much less affected by the polarity because the hydrocarbons of oil are non-polar and do not engage in Coulomb interactions with the polar chemical groups present on the solid surface. Oil molecules predominantly engage through London dispersion forces, both among themselves (cohesion interaction) and with the solid surface (adhesion interaction). Since in most cases dispersion-based cohesive and adhesive interactions are comparable, oil wets most surfaces very well, meaning that θ_o is very small.[74,75] A reasonable approximation[76] is thus to assume $\cos\theta_o = 1$ for all surface polarities. With that, eqn (8) simplifies to a direct relation between θ_{ow} and θ_w as

$$\cos\theta_{ow} = \frac{\gamma_w}{\gamma_{ow}}(\cos\theta_c - \cos\theta_w) \tag{9}$$

where we have introduced the *critical contact angle*, θ_c, which delineates the surface *wetting preference* for oil and water

$$\cos\theta_c = \frac{\gamma_o}{\gamma_w} \tag{10}$$

For liquid alkanes in the range from octane (C8) to hexadecane (C16), the surface tensions span from $\gamma_o = 22$ to 28 mN m^{-1},[70] which yields $\theta_c = 67^\circ$–73°. Fig. 3 shows the relation between the water contact angle (θ_w) and the w/o (left axis) and o/w (right axis) contact angles. The solid lines are predictions of eqn (9) for linear alkanes with lengths C8, C10, C12, and C16, based on experimental values for their respective surface tensions, γ_o and γ_{ow}.[70] In addition, the symbols are experimental data by Grate *et al.*[77] from direct w/o contact angle measurements on various silica and silanized silica surfaces, with hexadecane as the oil phase. We observe good agreement of our prediction, eqn (9), with the experimental data.

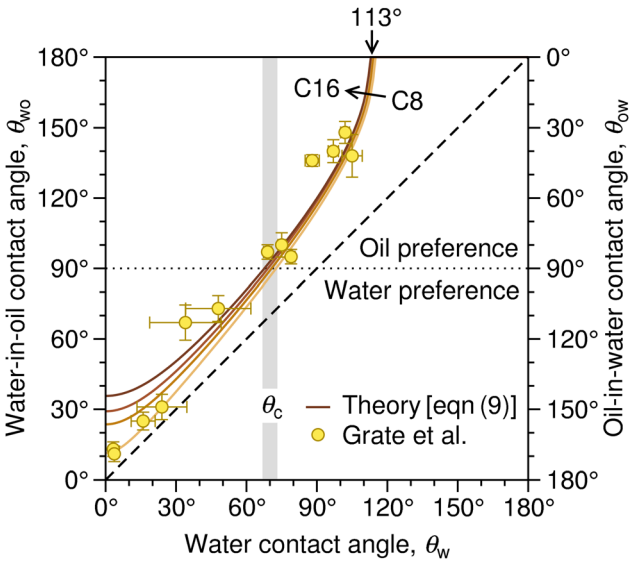

Fig. 3 Correlation between the water contact angle in air, θ_w, the water-in-oil contact angle, θ_{wo} (left axis), and the oil-in-water contact angle, θ_{ow} (right axis). The latter two are related as $\theta_{wo} + \theta_{ow} = 180^\circ$. The solid lines denote the prediction of eqn (9) based on the surface tension of a series of linear alkanes (C8, C10, C12, C16).[78,79] The symbols are contact angle measurements by Grate *et al.*[77] for water droplets on silica and silanized-silica surfaces in hexadecane. The diagonal dashed line denotes the symmetry $\theta_{wo} = \theta_w$. The gray stripe indicates the critical water contact angle in air, θ_c, at which θ_{ow} (and likewise θ_{wo}) reaches 90°, demarcating the border between the regime in which oil is favored for wetting the substrate (underwater oleophilicity) and the other regime in which water is favored (underwater oleophobicity).

The diagonal dashed line indicating the symmetry $\theta_{wo} = \theta_w$, serves as orientation. It is evident that water droplets have consistently larger contact angles in oil than in air, $\theta_{wo} > \theta_w$. In essence, oil competes with water for wetting the surface and thus reduces the wetting capability of water. Once θ_w surpasses

the value of around 113°, as indicated by an arrow in Fig. 3, water exhibits non-wetting behavior in oil (with $\theta_{wo} = 180°$ and $\theta_{ow} = 0$). A pivotal transition occurs at $\theta_{wo} = \theta_{ow} = 90°$, at which point the substrate exhibits identical wetting preference to oil and water. Based on eqn (9), this transition occurs at the critical contact angle of $\theta_w = \theta_c$, depicted as a gray stripe in Fig. 3. At the contact angle θ_c, the substrate switches from an effectively hydrophilic to effectively hydrophobic behavior under oil, even though it is conventionally classified as hydrophilic in air up to $\theta_w = 90°$. Concurrently, a surface is underwater olephobic for $\theta_w < \theta_c$, and underwater olephilic for $\theta_w > \theta_c$.

Notably, the critical contact angle for oil/water wetting preference, $\theta_c = 70° \pm 3°$ [eqn (10)], closely aligns with the Berg limit of $\theta_{adh} \approx 65° \pm 9°$, which denotes the threshold for the adhesion of macromolecules (Fig. 1a) and attraction between solid surfaces (Fig. 1b). We assert that the resemblance of the two values, $\theta_{adh} \approx \theta_c$, is not a mere coincidence. Instead, this striking correspondence can be understood from the notion that many relevant interaction scenarios can be viewed as three-phase contact problems comprising the surface in question, water, and a generic oil-like material. In the following, we will outline four interaction scenarios, which are sketched in Fig. 4. We will demonstrate that θ_w being above or below θ_c has profound implications on their behavior.

4 Critical contact angle as the adhesion threshold

We first address the adhesion threshold of macromolecules and cells to surfaces as shown in Fig. 1a. Within the context of biological adhesion, it is crucial to acknowledge that many macromolecules have amphiphilic structures. Examples include lipid aggregates and proteins in their native forms, which possess a hydrophobic core and a hydrophilic exterior. When such macromolecules or their aggregates encounter surfaces in aqueous settings, they can undergo reconfiguration and expose their hydrophobic regions to the surface. This adaptability significantly influences their adhesion properties.

4.1 Lipid monolayer adsorption

Lipids are the prototypical example of amphiphilic biological molecules. They can self-assemble into bilayers in water and form dense monolayers on hydrophobic surfaces, owing to their nonpolar tails. In our first example, we consider a two-state lipid layer model capable of either existing as a bilayer of surface area A in the bulk solution or as a monolayer with surface area $2A$ adsorbed on a solid substrate as depicted in Fig. 4a. An intriguing question arises: what contact angle of the substrate is necessary for stable lipid monolayers to nonspecifically adsorb to the surface from an aqueous medium? In other words, which of the two states, a non-adsorbed bilayer or an adsorbed monolayer, is thermodynamically favored?

A comprehensive thermodynamic analysis of this problem has been presented in our recent publication.[80] Here, we only briefly recap the main steps: first, we hypothetically separate both leaflets of the bilayer across vacuum, requiring the work Aw_{ll}, where w_{ll} represents the lipid–lipid (ll) monolayer adhesion tension in vacuum, analogous to w_{ss} in Section 2.3. Next, we remove the water from the substrate region of area $2A$ where the lipid monolayer will adsorb. The free energy cost for this water removal is $2A(\gamma_{sv} - \gamma_{sw}) = 2A\gamma_w \cos\theta_w$, where we used the Young equation [eqn (5)]. Finally, we attach the monolayer to the dry substrate, gaining the free energy of $-2Aw_{sl}$, where w_{sl} is

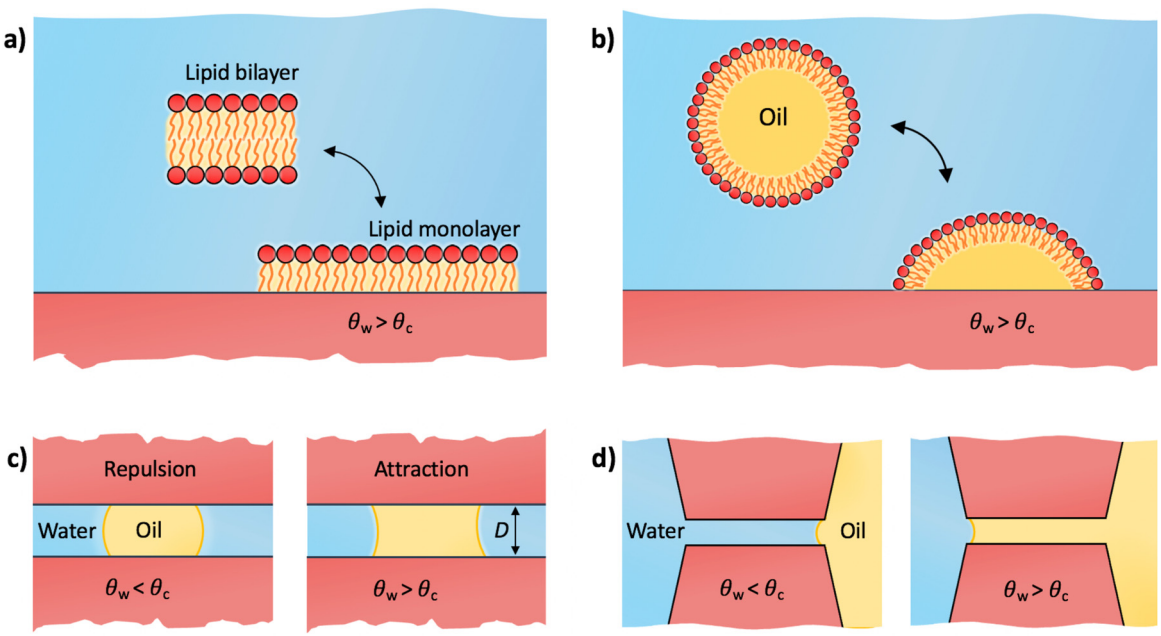

Fig. 4 Various scenarios that exhibit three-phase substrate–water–oil interactions. (a) Adsorption of a lipid monolayer. (b) Adsorption of a lipid-coated oil droplet. (c) Oil droplet bridging two similar parallel surfaces. (d) Competition between water and oil to imbibe a slit pore.

the substrate–lipid (sl) monolayer adhesion tension across vacuum. Summing up the three contributions provides us with the adsorption free energy per unit monolayer area

$$\Delta W/A = w_{ll} - 2w_{sl} + 2\gamma_w \cos\theta_w \quad (11)$$

While the first two adhesion terms were thoroughly examined through atomistic simulations,[80] here we provide a simple yet accurate estimation: lipid tails, being hydrocarbon-based and highly flexible with a liquid-like nature, can effectively be characterized as an oil-like medium. The work required to separate two leaflets is similar to creating two oil interfaces, such that $w_{ll} \approx 2\gamma_o$.[80] Additionally, the work needed to separate the tails (again approximated by oil) from the substrate is given by the Young–Dupré equation $w_{sl} = \gamma_o(1 + \cos\theta_o) \approx 2\gamma_o$. Here, we have assumed good oil-in-air wettability ($\cos\theta_o \approx 1$) for any kind of substrate type. Using these estimates for w_{ll} and w_{sl}, eqn (11) simplifies to,

$$\Delta W/A = 2\gamma_w \cos\theta_w - 2\gamma_o \quad (12)$$

Spontaneous monolayer adsorption is possible when $\Delta W < 0$, a condition met when the contact angle exceeds the adsorption threshold θ_{ads} given by

$$\cos\theta_{ads} = \frac{\gamma_o}{\gamma_w} \quad (13)$$

Notably, this value is given by the very same expression as the critical contact angle for oil/water wetting preference [eqn (10)], hence $\theta_{ads} = \theta_c$. The identical outcome arises from approximating lipid tails as oil-like. Even when considering a wider range of surface chemistries,[80] θ_{ads} remains constrained within a relatively narrow range of around 60°–70°, thus reinforcing the validity of eqn (13).

It is worth emphasizing the resemblance between the expression for the free energy of monolayer adsorption [eqn (12)] and that for dry adhesion between two identical solid surfaces in pure water [eqn (2)]. In the former, the surface interaction term ($2\gamma_o$) results from the dispersion interactions with lipid tails, whereas in the latter (w_{ss}), it pertains to the interaction between two identical surfaces. As we have already pointed out before, it is reasonable to assume $w_{ss} \geq 2\gamma_o$. However, at the transition contact angle, the surfaces are sufficiently non-polar and oil-like, therefore $w_{ss}(\theta_{adh}) \approx 2\gamma_o$, leading to similar results for the critical contact angles.

4.2 Adhesion of a lipid droplet

A variation to the lipid-monolayer adsorption scenario described in the previous subsection involves an oil droplet covered by a monolayer of insoluble surfactants (*e.g.*, lipids), referred to as a lipid droplet, illustrated in Fig. 4b. Lipid droplets are abundant in various organisms, where they function as structures for storing energy and as essential building blocks.[81,82] The technology behind lipid droplets also bears relevance in biofuel production and formulations for food and drug delivery.[83–85] The concept of a lipid droplet holds significance also for understanding various soft systems characterized by hydrophilic exteriors and nonpolar, hydrocarbon-rich interiors. At the most simplistic level, proteins may be conceptually grouped within this category. In spite of the intricate biophysics governing protein adsorption, influenced by diverse biological and physicochemical factors,[8,25] the minimal model of a lipid droplet can serve as a useful starting point for elucidating the Berg limit for non-specific adsorption of those proteins that strongly deform or even denature upon adsorption.[8]

As for the monolayer adsorption, a similar question arises here: for which substrate contact angles will a lipid droplet adhere to the substrate? The droplet adheres to the substrate by exposing its internal oil phase directly to the substrate while maintaining the lipid coating at its water interface. This reorganization creates a substrate–oil interface at the droplet's base of area A_{base}, which replaces the previous substrate–water interface in that area. The free energy change for modifying this interface is $A_{base}(\gamma_{so} - \gamma_{sw})$. The base area is influenced by the extent of the droplet's spread over the substrate, which is determined by the intricate interactions of lipids with both the oil phase and the substrate. While we will not delve into these specifics, our focus lies solely in assessing the onset of adhesion, regardless of the precise value of A_{base}. Using eqn (7), the free energy for droplet adhesion can be expressed as

$$\Delta W = -A_{base}\gamma_{ow}\cos\theta_{ow} \quad (14)$$

It follows that droplet adhesion, given by $\Delta W < 0$, is favorable for $\theta_{ow} < 90°$, which, using eqn (9), corresponds to $\theta_w > \theta_c$. This outcome is once again dictated by the critical angle for the oil/water wetting preference [eqn (10)].

The two specific examples of monolayer and lipid droplet adhesion can be seen as representatives of the broader phenomenon of adhesion of soft biological entities with hydrophobic oil-like interior and hydrophilic exterior. This concept clearly demonstrates that such particles follow the adhesion pattern shown in Fig. 1a, whereby the adhesion threshold is given by the critical contact angle for oil/water wetting preference, θ_c [eqn (10)].

5 Critical contact angle as the attraction threshold between similar surfaces

Let us now move on to the other question of this perspective, namely how to understand the adhesion threshold, θ_{adh}, as the onset of long-range attraction between two similar surfaces, as first pointed out by Vogler (Fig. 1b). As we discussed above, the long-range nature of the interaction cannot be explained by considering the surfaces in pure water alone. Rather, our explanation is based on the presence of an oil component. When a surface is submerged in water containing organic matter (particularly in natural waters, the bloodstream, or engineered aqueous systems), small and large organic molecules (*e.g.*, proteins, polysaccharides, and polymers) can rapidly accumulate on its interface, and form droplets or a liquid film.[33,86–92] It is important to note that even in purified water, traces of insoluble organic impurities tend to agglomerate on

surfaces in the form of nanodroplets.[93] A prominent example involves minute amounts of widely used silicone oils for laboratory equipment, which were shown to easily contaminate AFM tips.[94] This accumulated organic matter, referred to as the *conditioning film*, whether in the form of a uniform layer or as sessile droplets, profoundly influences subsequent adhesive events associated with the attachment of bacteria, cells, and other organisms, and it thus constitutes the initial stage of biofouling.[86–88] Adsorbed oil droplets can also stem from a surface that was pre-contaminated with nonpolar liquids. Once the surface is immersed in water, the liquid film can decompose into droplets.[95]

5.1 Bridging oil droplet

We now examine the impact of a small oil droplet (*e.g.*, a component of a conditioning film) bridging two chemically similar, uniform, and parallel surfaces characterized by a contact angle θ_w, as illustrated in Fig. 4c. The droplet exerts a capillary force on the surfaces. At small separations (smaller than the lateral extension of the droplet), this capillary force can be expressed as[71,96]

$$F = -\frac{2\gamma_{ow}V}{D^2}\cos\theta_{ow} + O\left(D^{-1/2}\right) \quad (15)$$

where V is the volume of the bridging droplet and D is the separation between the surfaces. The first term is the contribution due to the Laplace pressure and dominates over the second term, which includes contributions of the surface tension. A derivation and in-depth discussion on capillary forces can be found elsewhere.[71,96]

For $\theta_{ow} > 90^\circ$ (occurring for $\theta_w < \theta_c$), the force is repulsive ($F > 0$) at small separations. The force switches to attractive only for a very stretched droplet upon retraction of the surfaces, near the point of rupture (where higher-order terms in eqn (15) stemming from the surface tension dominate).[71] Conversely, if the o/w contact angle is below 90° (corresponding to $\theta_w > \theta_c$), the capillary force is always attractive ($F < 0$). This means that surfaces with contact angles above $\theta_w > \theta_c$ promote droplet-mediated attraction down to close-contact. This simple consideration underscores that oil nanodroplets play essentially a role similar to that of nanobubbles between hydrophobic surfaces. Just as gas nanobubbles can lead to long-range attraction between hydrophobic surfaces ($\theta_w > 90^\circ$), oil droplets are expected to engender attraction even between mildly hydrophilic surfaces with water contact angles down to θ_c. In simpler terms, the attraction between hydrophilic surfaces, which would occur only below around 1 nm in pure water (Section 2.3), can extend to longer ranges in the presence of oil droplets on the surfaces. The range and strength of this attraction crucially depend on the size and the amount of the droplets, similarly as in the case of nanobubbles. In essence, larger and more abundant oil droplets lead to stronger and longer-ranged attraction between the surfaces. This very mechanism could be the key explanation for the pronounced long-range attraction observed in certain experiments where the contact angles are below 90°.[17,64–66]

5.2 Wetting pores and slits

In the preceding subsection, we demonstrated that oil droplets can mediate long-range attraction between surfaces with contact angles exceeding 65°. Yet, the presence of oil can bring about other closely related practical effects, especially regarding the wetting of small pores. For illustration, we consider a continuous phase of oil in contact with a continuous phase of water, which both compete to wet a pore or a slit between two parallel surfaces (Fig. 4d). The free energy associated with oil displacing water in the slit is $\Delta W = 2A(\gamma_{so} - \gamma_{sw})$, where A is the surface area of the slit. By applying eqn (7), the free energy can be expressed as $\Delta W/A = -2\gamma_{ow}\cos\theta_{ow}$. For $\theta_{ow} > 90^\circ$ (corresponding to $\theta_w < \theta_c$), water will spontaneously wet the slit ($\Delta W > 0$). Conversely, for $\theta_{ow} < 90^\circ$ (corresponding to $\theta_w > \theta_c$), oil will displace water and imbibe the slit ($\Delta W < 0$).

In the broader context of aqueous systems, this simple calculation implies that a narrow slit with $\theta_w > \theta_c$ will favor wetting by oil. Such a slit will gradually accumulate organic material from its surroundings over time (akin to capillary condensation in hydrophilic pores), eventually leading to droplet-mediated attraction. Conversely, a more hydrophilic slit favoring wetting by water ($\theta_w < \theta_c$) will progressively expel organic material over time.

The scenarios outlined in this section, namely the bridging oil droplet and oil imbibition (Fig. 4c and d, respectively), offer a compelling explanation for the experimentally observed long-range attractive forces for surface contact angles above the Berg limit, as depicted in Fig. 1b. These scenarios feature a symmetrical boundary condition involving two identical solid surfaces with well-defined contact angles. In contrast, the macromolecular adhesion scenarios (highlighted in Fig. 4a and b) involve an adhering entity that does not have a well-defined contact angle but is amphiphilic and deformable. It is intriguing that despite these contrasting boundary conditions, the threshold contact angle is the same in all scenarios and related to the transition for oil/water wetting preference. The reason for this uniformity is that both kinds of scenarios can be perceived as three-phase contact problems, encompassing the surface under consideration, water, and a generic oil-like medium. As a result, the defining contact angle for adhesion/attraction is determined by the ratio between the surface tensions of oil and water, as given by eqn (10).

The competition between water and oil to imbibe tiny pores holds significant relevance across various technological domains, notably in secondary oil recovery, where hydrocarbons are extracted from fractured rock reservoirs using waterflooding techniques.[97,98] Moreover, biological or engineered water channels should be hydrophilic enough ($\theta_w < \theta_c$) to prevent the accumulation of organic material. A classic example of this principle can be found in porous membranes used for filtering emulsified oil droplets in wastewater treatment. To effectively prevent the passage of oil through the membrane pores and to mitigate its fouling, the membrane's contact angle should be less than 65°.[99] However, surfactants present in wastewater can alter the wetting behavior of oil droplets and render the membrane less hydrophilic. Therefore, additional

antifouling strategies are essential, such as surface hydrophilization, zwitterionic polymer coating, photocatalytic cleaning, and electrically enhanced antifouling.[99–101]

Finally, the displacement of one liquid by another within a pore can be associated with a free energy barrier, leading to kinetically trapped metastable states. Such metastability is used to design surfaces that exhibit both superhydrophobicity in oil and superoleophobicity in water, termed *dual superlyophobicity*. This unique property is achieved by a distinct topography of micro-sized pores.[102,103] When the surface is immersed in either oil or water, the liquid fills the pores. A droplet of the other liquid can then be placed on the surface without displacing the first liquid from the pores. The resulting metastable Cassie-type wetting state, characterized by a large apparent contact angle, is mechanically stable if the intrinsic contact angle of the surface material lies in a narrow range around 65°, where the difference in wetting affinities between oil and water is small.

6 Conclusions

In this perspective, our central discussion revolved around understanding the reasons for the observed long-range attraction and adhesion tendencies exhibited by surfaces with contact angles ranging from approximately 65° to 90°. We rationalized these observations by recognizing that the attractive and adhesive properties stem from nonpolar, hydrophobic components within interacting entities in aqueous systems. These hydrophobic components can manifest in various forms, whether in the shape of tiny liquid nanodroplets or as constituents within deformable hydrophobic parts of soft biological matter.

In all the examined scenarios, adhesion sets in when the solid surface displays an *underwater oleophilic* character, which is equivalent to being *underoil hydrophobic*. This character emerges when the contact angle surpasses a critical value of $\theta_c = 70^\circ \pm 3^\circ$ and is determined by the ratio between the surface tensions of oil and water. Importantly, this critical value closely aligns with the experimentally observed Berg limit for the adhesion threshold of biomatter, $\theta_{adh} \approx 65^\circ \pm 9^\circ$.

Our discussion on nonspecific adhesion was based on a minimalist model, focusing on flat and featureless surfaces in the presence of an oil-like component in water. However, real-world systems can bring about a host of complexities. For instance, the hydrophobic component may contain heteroatoms, leading to increased polarity compared to purely nonpolar oils. Additionally, surfaces with pronounced topographical features can give rise to additional wetting states,[27,104] some of which may even be metastable.[102,103] Highly charged or highly polarizable surfaces, such as metals, bring additional interactions that may facilitate or hinder adhesion.[105,106] Each of the scenarios discussed above will thereby become more specific and intricate, accompanied by a myriad of other factors. These complexities underscore the fact that the adsorption threshold across different experiments is not sharp but rather consists of a narrow window that accommodates most practical cases.

Author contributions

MK: conceptualization, formal analysis, writing – original draft; ES: conceptualization, writing – original draft; RRN: conceptualization, writing – original draft.

Conflicts of interest

No conflicts of interest to disclose.

Acknowledgements

M. K. acknowledges financial support from the Slovenian Research and Innovation Agency ARIS (contracts P1-0055 and J1-4382). Funded by the Deutsche Forschungsgemeinschaft (DFG, German Research Foundation) – Project ID 431232613 – SFB 1449 and Project ID 387284271 – SFB 1349.

Notes and references

1 E. E. Meyer, K. J. Rosenberg and J. Israelachvili, *Proc. Natl. Acad. Sci. U. S. A.*, 2006, **103**, 15739–15746.
2 B. Geiger, J. P. Spatz and A. D. Bershadsky, *Nat. Rev. Mol. Cell Biol.*, 2009, **10**, 21–33.
3 D. Horinek, A. Serr, M. Geisler, T. Pirzer, U. Slotta, S. Q. Lud, J. A. Garrido, T. Scheibel, T. Hugel and R. R. Netz, *Proc. Natl. Acad. Sci. U. S. A.*, 2008, **105**, 2842–2847.
4 H. D. Follmann, A. F. Martins, A. P. Gerola, T. A. Burgo, C. V. Nakamura, A. F. Rubira and E. C. Muniz, *Biomacromolecules*, 2012, **13**, 3711–3722.
5 F. Persson, J. Fritzsche, K. U. Mir, M. Modesti, F. Westerlund and J. O. Tegenfeldt, *Nano Lett.*, 2012, **12**, 2260–2265.
6 G. J. Ma, B. K. Yoon, T. N. Sut, K. Y. Yoo, S. H. Lee, W.-Y. Jeon, J. A. Jackman, K. Ariga and N.-J. Cho, *View*, 2022, **3**, 20200078.
7 I. Eshet, V. Freger, R. Kasher, M. Herzberg, J. Lei and M. Ulbricht, *Biomacromolecules*, 2011, **12**, 2681–2685.
8 S. P. Mitra, *J. Surf. Sci Technol.*, 2020, **36**, 7–38.
9 M. M. van Schooneveld, E. Vucic, R. Koole, Y. Zhou, J. Stocks, D. P. Cormode, C. Y. Tang, R. E. Gordon, K. Nicolay and A. Meijerink, *et al.*, *Nano Lett.*, 2008, **8**, 2517–2525.
10 A. Luchini and G. Vitiello, *Front. Chem.*, 2019, **7**, 343.
11 Y. Wu, F. I. Simonovsky, B. D. Ratner and T. A. Horbett, *J. Biomed. Mater. Res., Part A*, 2005, **74**, 722–738.
12 L. Zhang, B. Casey, D. K. Galanakis, C. Marmorat, S. Skoog, K. Vorvolakos, M. Simon and M. H. Rafailovich, *Acta Biomater.*, 2017, **54**, 164–174.
13 V. A. Parsegian, N. Fuller and R. P. Rand, *Proc. Natl. Acad. Sci. U. S. A.*, 1979, **76**, 2750–2754.
14 J. N. Israelachvili and R. M. Pashley, *Nature*, 1983, **306**, 249–250.
15 E. Schneck, F. Sedlmeier and R. R. Netz, *Proc. Natl. Acad. Sci. U. S. A.*, 2012, **109**, 14405–14409.

16 J. L. Parker, P. M. Claesson and P. Attard, *J. Phys. Chem.*, 1994, **98**, 8468–8480.
17 E. A. Vogler, *Adv. Colloid Interface Sci.*, 1998, **74**, 69–117.
18 J. M. Berg, L. T. Eriksson, P. M. Claesson and K. G. N. Borve, *Langmuir*, 1994, **10**, 1225–1234.
19 M. Navarro, E. Engel, J. A. Planell, I. Amaral, M. Barbosa and M. Ginebra, *J. Biomed. Mater. Res., Part A*, 2008, **85**, 477–486.
20 N. Schwierz, D. Horinek, S. Liese, T. Pirzer, B. N. Balzer, T. Hugel and R. R. Netz, *J. Am. Chem. Soc.*, 2012, **134**, 19628–19638.
21 L. Peng, H. Li and Y. Meng, *Appl. Surf. Sci.*, 2017, **401**, 25–39.
22 E. A. Vogler, *J. Biomater. Sci., Polym. Ed.*, 1999, **10**, 1015–1045.
23 A. Sethuraman, M. Han, R. S. Kane and G. Belfort, *Langmuir*, 2004, **20**, 7779–7788.
24 P. Parhi, A. Golas and E. A. Vogler, *J. Adhes. Sci. Technol.*, 2010, **24**, 853–888.
25 E. A. Vogler, *Biomaterials*, 2012, **33**, 1201–1237.
26 Y. Tian and L. Jiang, *Nat. Mater.*, 2013, **12**, 291–292.
27 M. Liu, S. Wang and L. Jiang, *Nat. Rev. Mater.*, 2017, **2**, 1–17.
28 M. F. Ismail, M. A. Islam, B. Khorshidi, A. Tehrani-Bagha and M. Sadrzadeh, *Adv. Colloid Interface Sci.*, 2022, **299**, 102524.
29 A. Marmur, C. Della Volpe, S. Siboni, A. Amirfazli and J. W. Drelich, *Surf. Innov.*, 2017, **5**, 3–8.
30 J. Israelachvili and R. Pashley, *Nature*, 1982, **300**, 341–342.
31 J. Israelachvili and R. Pashley, *J. Colloid Interface Sci.*, 1984, **98**, 500–514.
32 S. Schilp, A. Kueller, A. Rosenhahn, M. Grunze, M. E. Pettitt, M. E. Callow and J. A. Callow, *Biointerphases*, 2007, **2**, 143–150.
33 A. Rosenhahn, S. Schilp, H. J. Kreuzer and M. Grunze, *Phys. Chem. Chem. Phys.*, 2010, **12**, 4275–4286.
34 R. Godawat, S. N. Jamadagni and S. Garde, *Proc. Natl. Acad. Sci. U. S. A.*, 2009, **106**, 15119–15124.
35 A. J. Patel, P. Varilly and D. Chandler, *J. Phys. Chem. B*, 2010, **114**, 1632–1637.
36 M. Kanduč, A. Schlaich, E. Schneck and R. R. Netz, *Adv. Colloid Interface Sci.*, 2014, **208**, 142–152.
37 N. B. Rego and A. J. Patel, *Annu. Rev. Condens. Matter Phys.*, 2022, **13**, 303–324.
38 D. Berard, P. Attard and G. Patey, *J. Chem. Phys.*, 1993, **98**, 7236–7244.
39 K. Lum, D. Chandler and J. D. Weeks, *J. Phys. Chem. B*, 1999, **103**, 4570–4577.
40 D. Bratko, R. A. Curtis, H. W. Blanch and J. M. Prausnitz, *J. Chem. Phys.*, 2001, **115**, 3873–3877.
41 X. Huang, C. J. Margulis and B. J. Berne, *Proc. Natl. Acad. Sci. U. S. A.*, 2003, **100**, 11953–11958.
42 D. Chandler, *Nature*, 2005, **437**, 640–647.
43 N. Choudhury and B. M. Pettitt, *J. Am. Chem. Soc.*, 2007, **129**, 4847–4852.
44 S. Sharma and P. G. Debenedetti, *Proc. Natl. Acad. Sci. U. S. A.*, 2012, **109**, 4365–4370.
45 K. Lum and D. Chandler, *Int. J. Thermophys.*, 1998, **19**, 845–855.
46 X. Huang, C. J. Margulis and B. J. Berne, *Proc. Natl. Acad. Sci. U. S. A.*, 2003, **100**, 11953–11958.
47 N. Choudhury and B. M. Pettitt, *J. Am. Chem. Soc.*, 2005, **127**, 3556–3567.
48 S. Sharma and P. G. Debenedetti, *Proc. Natl. Acad. Sci. U. S. A.*, 2012, **109**, 4365–4370.
49 P. Setny, Z. Wang, L.-T. Cheng, B. Li, J. McCammon and J. Dzubiella, *Phys. Rev. Lett.*, 2009, **103**, 187801.
50 P. Setny, R. Baron, P. Michael Kekenes-Huskey, J. A. McCammon and J. Dzubiella, *Proc. Natl. Acad. Sci. U. S. A.*, 2013, **110**, 1197–1202.
51 D. Bratko, R. Curtis, H. Blanch and J. Prausnitz, *J. Chem. Phys.*, 2001, **115**, 3873–3877.
52 R. Mehrani and S. Sharma, *J. Phys. Chem. B*, 2022, **126**, 5110–5116.
53 H. K. Christenson and P. M. Claesson, *Science*, 1988, **239**, 390–392.
54 D. J. Mastropietro and W. A. Ducker, *Phys. Rev. Lett.*, 2012, **108**, 106101.
55 S.-T. Lou, Z.-Q. Ouyang, Y. Zhang, X.-J. Li, J. Hu, M.-Q. Li and F.-J. Yang, *J. Vac. Sci. Technol., B: Nanotechnol. Microelectron.: Mater., Process., Meas., Phenom.*, 2000, **18**, 2573–2575.
56 N. Ishida, T. Inoue, M. Miyahara and K. Higashitani, *Langmuir*, 2000, **16**, 6377–6380.
57 J. Tyrrell and P. Attard, *Langmuir*, 2002, **18**, 160–167.
58 P. S. Epstein and M. S. Plesset, *J. Chem. Phys.*, 1950, **18**, 1505–1509.
59 D. Lohse and X. Zhang, *Phys. Rev. E: Stat., Nonlinear, Soft Matter Phys.*, 2015, **91**, 031003.
60 D. Lohse and X. Zhang, *Rev. Mod. Phys.*, 2015, **87**, 981.
61 B. H. Tan, H. An and C.-D. Ohl, *Phys. Rev. Lett.*, 2018, **120**, 164502.
62 B. H. Tan, H. An and C.-D. Ohl, *Phys. Rev. Lett.*, 2019, **122**, 134502.
63 R.-H. Yoon and S. Ravishankar, *J. Colloid Interface Sci.*, 1996, **179**, 391–402.
64 M. Hato, *J. Phys. Chem.*, 1996, **100**, 18530–18538.
65 N. Ishida, N. Kinoshita, M. Miyahara and K. Higashitani, *J. Colloid Interface Sci.*, 1999, **216**, 387–393.
66 R. F. Considine and C. J. Drummond, *Langmuir*, 2000, **16**, 631–635.
67 M. Kanduč, E. Schneck and R. R. Netz, *Chem. Phys. Lett.*, 2014, **610**, 375–380.
68 M. Kanduč and R. R. Netz, *Proc. Natl. Acad. Sci. U. S. A.*, 2015, **112**, 12338–12343.
69 M. Kanduč, A. Schlaich, E. Schneck and R. R. Netz, *Langmuir*, 2016, **32**, 8767–8782.
70 O. Ozkan and H. Y. Erbil, *Surf. Topogr.*, 2017, **5**, 024002.
71 E. De Souza, M. Brinkmann, C. Mohrdieck, A. Crosby and E. Arzt, *Langmuir*, 2008, **24**, 10161–10168.
72 Y. Uematsu, D. J. Bonthuis and R. R. Netz, *Curr. Opin. Electrochem.*, 2019, **13**, 166–173.
73 F. Bartell and H. Osterhof, *Ind. Eng. Chem. Res.*, 1927, **19**, 1277–1280.

74 B. T. Ingram, *J. Chem. Soc., Faraday Trans.*, 1974, **70**, 868–876.
75 B. Janczuk, *Fuel*, 1986, **65**, 113–116.
76 M. I. J. van Dijke and K. S. Sorbie, *J. Pet. Sci. Eng.*, 2002, **33**, 39–48.
77 J. W. Grate, K. J. Dehoff, M. G. Warner, J. W. Pittman, T. W. Wietsma, C. Zhang and M. Oostrom, *Langmuir*, 2012, **28**, 7182–7188.
78 J. J. Jasper and E. V. Kring, *J. Phys. Chem.*, 1955, **59**, 1019–1021.
79 A. Goebel and K. Lunkenheimer, *Langmuir*, 1997, **13**, 369–372.
80 M. Šako, F. Staniscia, E. Schneck, R. R. Netz and M. Kanduč, *PNAS Nexus*, 2023, **2**, pgad190.
81 T. C. Walther and R. V. Farese Jr, *Biochim. Biophys. Acta, Mol. Cell Biol. Lipids*, 2009, **1791**, 459–466.
82 A. R. Thiam, R. V. Farese Jr and T. C. Walther, *Nat. Rev. Mol. Cell Biol.*, 2013, **14**, 775–786.
83 S. S. Okubanjo, S. M. Loveday, A. Ye, P. J. Wilde and H. Singh, *J. Agric. Food Chem.*, 2019, **67**, 2626–2636.
84 J. A. Julien, A. L. Pellett, S. S. Shah, N. J. Wittenberg and K. J. Glover, *Biochim. Biophys. Acta, Biomembr.*, 2021, **1863**, 183624.
85 J. Musakhanian, J.-D. Rodier and M. Dave, *AAPS PharmSciTech*, 2022, **23**, 151.
86 M. E. Callow and R. L. Fletcher, *Int. Biodeterior.*, 1994, **34**, 333–348.
87 S. Abarzua and S. Jakubowski, *Mar. Ecol. Prog.*, 1995, **123**, 301–312.
88 D. M. Yebra, S. Kiil and K. Dam-Johansen, *Prog. Org. Coat.*, 2004, **50**, 75–104.
89 S. Hong and M. Elimelech, *J. Membr. Sci.*, 1997, **132**, 159–181.
90 A. Armanious, M. Aeppli and M. Sander, *Environ. Sci. Technol.*, 2014, **48**, 9420–9429.
91 Y.-M. Lin, C. Song and G. C. Rutledge, *ACS Appl. Mater. Interfaces*, 2019, **11**, 17001–17008.
92 K. Park, D. Lee, J.-H. Lim, J. Hong and G. Lim, *Langmuir*, 2022, **38**, 9884–9891.
93 R. P. Berkelaar, E. Dietrich, G. A. Kip, E. S. Kooij, H. J. Zandvliet and D. Lohse, *Soft Matter*, 2014, **10**, 4947–4955.
94 Y.-S. Lo, N. D. Huefner, W. S. Chan, P. Dryden, B. Hagenhoff and T. P. Beebe, *Langmuir*, 1999, **15**, 6522–6526.
95 D. Daniel, J. V. Timonen, R. Li, S. J. Velling and J. Aizenberg, *Nat. Phys.*, 2017, **13**, 1020–1025.
96 E. De Souza, L. Gao, T. McCarthy, E. Arzt and A. Crosby, *Langmuir*, 2008, **24**, 1391–1396.
97 S. Al-Anssari, A. Barifcani, S. Wang, L. Maxim and S. Iglauer, *J. Colloid Interface Sci.*, 2016, **461**, 435–442.
98 M. A. Q. Siddiqui, S. Ali, H. Fei and H. Roshan, *Earth-Sci. Rev.*, 2018, **181**, 1–11.
99 S. Huang, R. H. Ras and X. Tian, *Curr. Opin. Colloid Interface Sci.*, 2018, **36**, 90–109.
100 N. Ismail, W. Salleh, A. Ismail, H. Hasbullah, N. Yusof, F. Aziz and J. Jaafar, *Sep. Purif. Technol.*, 2020, **233**, 116007.
101 Z. He, X. Lan, Q. Hu, H. Li, L. Li and J. Mao, *Prog. Org. Coat.*, 2021, **157**, 106285.
102 X. Tian, V. Jokinen, J. Li, J. Sainio and R. H. Ras, *Adv. Mater.*, 2016, **28**, 10652–10658.
103 M. Liu, L. Tie, J. Li, Y. Hou and Z. Guo, *J. Mater. Chem. A*, 2018, **6**, 1692–1699.
104 Y. Tian, B. Su and L. Jiang, *Adv. Mater.*, 2014, **26**, 6872–6897.
105 H. Singh and S. Sharma, *Mol. Simul.*, 2021, **47**, 420–427.
106 A. F. Qadikolae and S. Sharma, *J. Mol. Liq.*, 2023, **379**, 121685.